11
Quantitative EXAFS Analysis

Bruce Ravel

National Institute of Standards and Technology, Gaithersburg, MD, USA

Analysis of the extended x-ray-absorption fine-structure (EXAFS) provides fine details of the partial pair distribution functions of atoms surrounding the absorber, including distances, mean square deviations in distance, coordination numbers, and coordinating species. Because neither the theory nor the interpretation of the EXAFS makes any assumption of configurational symmetry or periodicity, EXAFS is equally applicable to all forms of condensed matter. Because the basic physical process of x-ray absorption spectroscopy (XAS), the photo-excitation of a deep core electron, is element specific, EXAFS is applicable even to dilute systems. Consequently, EXAFS plays a valuable role in a wide variety of scientific disciplines, with applications in life science, earth and environmental science, chemistry, materials science, cultural heritage, and more. In short, EXAFS is one of the core competencies of any synchrotron radiation facility.

The obvious first question is how to distinguish the x-ray-absorption near-edge structure (XANES) from the EXAFS. From a real-space, multiple-scattering point of view, there is no obvious distinction. The photo-excitation in XAS is an example of Fermi's golden rule, wherein a dipole interaction (the incident photon) mediates the promotion of an electron from its initial, deep-core state into an unoccupied, high-lying state. That is true at all energies and at all energies there is a formal solution to Fermi's golden rule involving multiple-scattering theory. So, how, *in practice*, do we distinguish XANES from EXAFS?

The theory of the real-space, multiple-scattering formalism [1–3] involves a substantial amount of linear algebra. It is possible to define a mathematical distinction between XANES and EXAFS on the basis of the mathematical properties [4, 5] of one particular matrix used in the real-space, multiple-scattering approach. As an example, in copper metal, this strict mathematical criterion defining the XANES region extends to about 16 eV above the edge or about 2 Å^{-1} in photoelectron wavenumber. While this may be a rigorous definition of the boundary between XANES and EXAFS, it is not a very *practical* one.

In practice, the EXAFS region is chosen to begin 25 eV to 35 eV above the edge, or about 2.5 Å^{-1} to 3 Å^{-1}. This is a useful rule of thumb. It is an energy where the formal solution is convergent as a path expansion. The photoelectron has enough kinetic energy that it is relatively insensitive to the computational details of

X-Ray Absorption and X-Ray Emission Spectroscopy: Theory and Applications, First Edition.
Edited by Jeroen A. van Bokhoven and Carlo Lamberti.

the potential model used in the theory. Finally, it is far enough away from the edge that common background removal algorithms [6–10] are stable and reliable. In short, the definition of the EXAFS region used in this chapter is the region of the XAS spectrum for which EXAFS analysis can be performed reliably.

11.1 A brief history of EXAFS theory

EXAFS as an analytic tool began with the seminal 1971 paper by Sayers, Stern, and Lytle [11]. A later paper [12] outlined the basic data processing steps still used today. The slowly varying background function is subtracted from the measured absorption data, isolating the fine structure $\chi(E)$. The energy axis is converted to photoelectron wavenumber, k, and $\chi(k)$ is subjected to a complex Fourier transform. The complex $\tilde{\chi}(R)$ data, which resemble a pair distribution function, are interpreted to yield quantitative information about the local configuration environment around the absorbing atom.

Early quantitative approaches to analysis of the fine structure were purely empirical and mostly involved spectral filtering. That is, the $|\tilde{\chi}(R)|$ data are windowed around a peak in the low-R region and subjected to a reverse Fourier transform. This isolates the contribution to $\chi(k)$ from a narrow band in frequency, thus isolating the signal from a near-neighbor coordination shell.

This Fourier filtered data was used in several ways to extract quantitative structural information from early EXAFS measurements. Each of these strategies requires that the signal from a coordination shell be isolated from the rest of the signal. Isolated signals from a well-known standard were used as fitting standards. In Ref. [13], the first shell signal in bulk InP was used as the fitting standard to measure the effect of strain in InP thin films. A second approach, the so-called "log-ratio" method [14], would fit polynomials to ratio and difference spectra computed from Fourier filtered data of a known standard and an unknown sample. The terms of the polynomials are related to changes in coordination number, distance, and σ^2. A third approach [15] would reconstruct a partial pair distribution function by fitting a cumulant expansion to Fourier filtered data, subject to certain constraints on the distribution function.

While each approach was used successfully for years, the Fourier filtering techniques all share serious shortcomings. They require that the contribution from a coordination shell be amenable to spectral isolation. Consider Fig. 11.1, which shows the Fourier transformed $|\tilde{\chi}(R)|$ for body-centered-cubic (BCC) iron metal measured at 60 K along with the Fourier transforms of the fitted contributions from the two nearest neighbor coordination shells – 8 iron scatterers at 2.477(5) Å and 6 at 2.860(6) Å. These two signals overlap substantially. Even though the BCC structure is simple and well-ordered, an analytic technique relying on spectral isolation of shells will fail. That is the case for most materials beyond the first coordination shell. A second pitfall to filtering techniques is that they demand measurement of a suitable standard, something which may not exist for a sample away from thermodynamic equilibrium or which contains an unusual absorber/scatterer pair.

During this early period, much progress was made towards a formal, theoretical understanding of EXAFS [16, 17] as well as a practical, semi-empirical formulation [18] that we have come to call the "EXAFS equation". The contribution from an individual scattering atom (or, as explained below, from a multiple scattering path), Γ, is given by

$$\chi_\Gamma(k) = \frac{S_0^2 N_\Gamma F_\Gamma(k)}{2kR_\Gamma^2}\, e^{-2k^2\sigma_\Gamma^2}\, e^{-R_\Gamma/\lambda_\Gamma(k)}\, \sin(2kR_\Gamma + \delta_\Gamma(k)) \tag{11.1}$$

$$\chi(k|\mathsf{theory}) = \sum_\Gamma \chi_\Gamma(k) \tag{11.2}$$

and the full theoretical calculation is given by the sum over all scattering atoms (and multiple scattering paths).

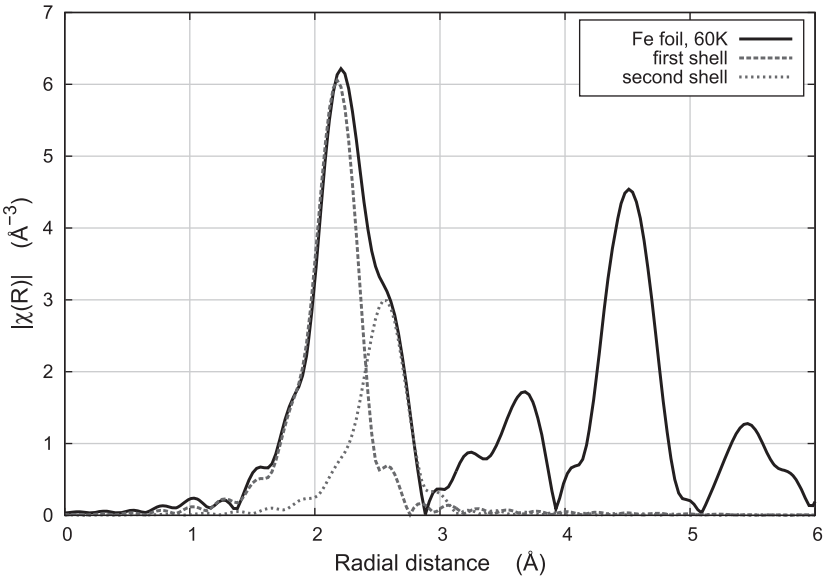

Figure 11.1 *Overlapping contributions from the first two shells in iron metal.*

Table 11.1 *The terms in the EXAFS equation. E_0 is a parameter which aligns the energy grid of the calculation to the energy grid of the data. $R_{0,\Gamma}$ is the half-path length from the input configuration and ΔR_Γ is the deviation from $R_{0,\Gamma}$ determined by the analysis.*

parameter	description	source	relation
k	photoelectron wavenumber		$k = \frac{\hbar}{2m_e}\sqrt{(E - E_0)}$
$F_\Gamma(k)$	effective scattering amplitude	theory	
$\delta_\Gamma(k)$	central + scattering atom phase shift	theory	
$\lambda_\Gamma(k)$	photoelectron mean free path	theory	
S_0^2	amplitude reduction factor	modeled	
N_Γ	path degeneracy	modeled	
σ_Γ^2	mean square deviation in half path length	modeled	
R_Γ	half path length	modeled	$R_\Gamma = R_{0,\Gamma} + \Delta R_\Gamma$

The EXAFS signal, therefore is related to the terms of the local configuration environment and to the complex function which describes the scattering of the photoelectron from the surrounding atoms. This equation explains many of the basic physical characteristics of the EXAFS measurement. The fine structure is oscillatory due to the sinusoidal dependence upon inter-atomic distance R. EXAFS is a local structure probe due to the effect of the photoelectron mean free path, λ, in the $e^{-R/\lambda(k)}/R$ term. Each term is explained in Table 11.1. For an excellent, semi-empirical derivation of the EXAFS equation, the reader is referred to Ref. [19].

By the middle part of the 1990s, there were three user-oriented theory packages which enabled the application of high quality theory to EXAFS data analysis: EXCURVE [20], GNXAS [21], and FEFF [22], each of which developed a wide user base and contributed substantively to the development of EXAFS as a practicable measurement technique. The three packages share certain similarities. Each uses a cluster

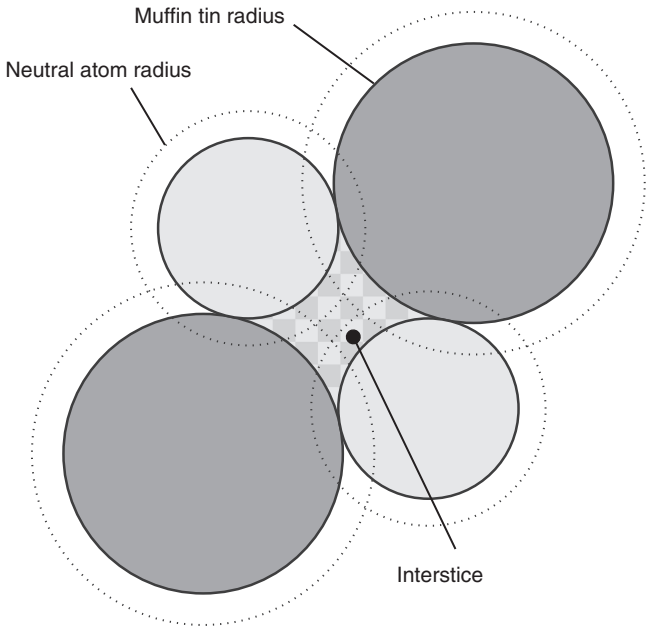

Figure 11.2 *A schematic, redrawn from Ref. [28], of the geometry of the muffin tin potential. Source: Pauli, 1999, [28]. Reproduced with permission from M. Pauli.*

expansion to represent the EXAFS signal as a sum of geometric contributions and each computes scattering potentials using a muffin tin formalism.

The muffin tin (MT) potential is an old idea [23] first introduced as a way of solving problems of electron motion in periodic potentials. A thorough overview of its use in EXAFS is given in Sec. II.B.1 of Ref. [24]. As shown schematically in Fig. 11.2, each atom is represented by a sphere which just touches neighboring atoms or is slightly overlapped. [25] The interstice, the space between the spheres, is flat and of uniform charge density. From this potential surface, scattering amplitudes and phase shifts are calculated.

It is not obvious that the MT potential could be a successful basis for EXAFS analysis. A chemical bond implies both a break from spherical symmetry and variable electron density within the interstice. Recent developments [26, 27] in the computation of the near edge structure have clearly demonstrated that non-MT potentials are essential to accurately replicate XANES spectra. However, far above the absorption edge, the photoelectron has sufficient kinetic energy that it is mostly insensitive to the details of the potential surface. The MT potential remains common and useful for EXAFS applications.

The earliest attempts [29] to provide a practical theory for EXAFS analysis made several significant approximations. Among these was the treatment of the photoelectron as a plane wave rather than as an outwardly propagating spherical wave. This is a reasonable approximation when the kinetic energy of the photoelectron is large enough that the curvature of the spherical wave can be neglected. For an EXAFS signal dominated by signal at low photoelectron wavenumber, either due to large σ^2 in Eq. (11.1) or to the nature of $F(k)$ of the scattering atom, this is a poor approximation. Each of the three theory program implements a curved-wave approach.

Other significant improvements to the calculation of theoretical scattering factors were made in the period between the 1970s and the mid-1990s. These included an effective treatment of intrinsic losses [30], typically included in Eq. (11.1) by the S_0^2 term, and of the quantum mechanical, many-body, exchange correlations. The latter yields an energy dependent self-energy, which has an impact on the evaluation of $\delta(k)$ in Eq. (11.1)

and therefore of the evaluation of R in the analysis of the EXAFS. The reader is refered to Refs. [24] and [21] for further discussion.

Given the MT description of the potential surface along with a curved-wave theory and ways of handling intrinsic losses and many-body effects, the next step is to perform some kind of cluster expansion within the context of real-space multiple-scattering theory. While a full derivation of the multiple scattering formalism as it is applied to EXAFS is beyond the scope of this chapter, an overview of the most salient points helps put the problem in proper context.

The process by which a photon is absorbed by an atom and a deep-core electron is photo-excited is an example of Fermi's Golden Rule:

$$\mu(E) \propto \sum_f \left|\langle f|\hat{\epsilon}\cdot\mathbf{r}|i\rangle\right|^2 \delta(\omega_f - \omega_i - E). \tag{11.3}$$

Here, $\mu(E)$ is the absorption cross-section as a function of incident photon energy, the very thing measured in absorption spectroscopy and the thing whose oscillatory structure we analyze in EXAFS. $|i\rangle$ and $|f\rangle$ are the initial (deep-core) and final (photo-excited) states of the electron. The transition between the states is mediated by a dipole interaction, $\hat{\epsilon}\cdot\mathbf{r}$. Finally, the Kronecker delta function restricts the evaluation of the equation to final states of the correct kinetic energy.

There are, in the broadest possible sense, two strategies for computing this function. One could represent the initial and final states and directly evaluate the integral implied by the bra-ket notation. More useful for EXAFS is to solve Eq. (11.3) using the Green's function for the Hamiltonian associated with the MT potential. With the operator associated with this Green's function, $\sum_f |f\rangle\mathbb{G}\langle f|$, the expression for $\mu(E)$ is rewritten as

$$\mu(E) \propto \langle i|\hat{\epsilon}^*\cdot\mathbf{r}\,\mathbb{G}(\mathbf{r},\mathbf{r}';E)\,\hat{\epsilon}\cdot\mathbf{r}'|i\rangle\Theta(E-E_F) \tag{11.4}$$

where Θ is a broadened Heaviside step function assuring that $\mu(E)$ is non-zero only above the Fermi energy, i.e. only for incident photon energies which can promote a deep core electron into an unfilled state.

$\mathbb{G}$ is the one-electron propagator function in the presence of the MT potential. That means that $\mathbb{G}$ describes all possible ways that the photo-electron can propagate away from the absorber and scatter from the surrounding atoms. $\mathbb{G}$ can be expressed in a series expansion as

$$\mathbb{G} = \mathsf{G}_0 + \mathsf{G}_0\mathsf{T}\mathsf{G}_0. \tag{11.5}$$

Here T, the atomic scattering matrix [2, 31], is expressed in terms of the single atom scattering matrix t as

$$\mathsf{T} = \mathsf{t} + \mathsf{t}\mathsf{G}_0\mathsf{t} + \mathsf{t}\mathsf{G}_0\mathsf{t}\mathsf{G}_0\mathsf{t} + \cdots. \tag{11.6}$$

Substituting this into Eq. (11.5) yields

$$\mathbb{G} = \mathsf{G}_0 + \mathsf{G}_0\mathsf{t}\mathsf{G}_0 + \mathsf{G}_0\mathsf{t}\mathsf{G}_0\mathsf{t}\mathsf{G}_0 + \mathsf{G}_0\mathsf{t}\mathsf{G}_0\mathsf{t}\mathsf{G}_0\mathsf{t}\mathsf{G}_0 + \cdots \tag{11.7}$$

Eq. (11.7) is the starting point for EXAFS analysis. The matrix G_0 is the free electron propagator, which describes the ways an electron can travel from one point in space to another. t is the single atom scattering matrix. It describes how an electron scatters from each atom in the cluster. The second term in Eq. (11.7) describes all the ways the photoelectron propagates away from the absorber and scatters exactly once from a surrounding atom. The third term describes all the ways the photoelectron scatters twice, propagating between and scattering from two other atoms in the cluster. The following terms describe successively higher orders of scattering. At each order of Eq. (11.7), scattering is considered from all atoms in the cluster used to compute the MT potential.

By itself, Eq. (11.7) is not especially useful. Each of the three theory programs further expands each term of Eq. (11.7) into a series of scattering configurations. How this expansion is implemented is a substantial distinction between the three popular theory programs. However, each of the theory programs implemented several features essential to quantitative analysis of the EXAFS data.

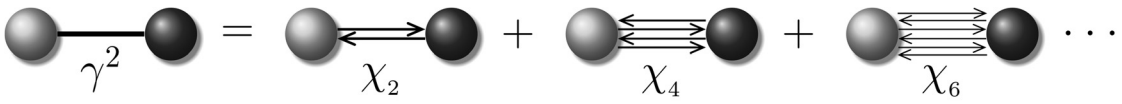

Figure 11.3 *Pictorial depiction of* GNXAS' *γ^2 signal. The light gray ball represents the absorber, the dark gray ball is another atom in the cluster. The path of the photoelectron is indicated by the arrows for each order of scattering. This was redrawn from figure 1 in Ref. [21]. Source: Filipponi, et al., 1995, [21]. Reproduced with permission from American Physical Society and A. Filipponi.*

11.1.1 The n-body decomposition in GNXAS

GNXAS performs what its authors call an *n-body decomposition* of the Green's function in Eq. (11.5). Given the cluster of atoms from which the MT potentials were computed, the program considers sub-clusters of atoms with 1, 2, or more atoms along with the absorbing atom. For each n-atom configuration, Eq. (11.5), i.e. scattering to all orders within that sub-cluster, is calculated. For a two atom sub-cluster, this is called the γ^2 signal and is shown schematically in Fig. 11.3. The γ^2 signal from an absorber/scatterer pair includes the single scattering contribution (χ_2), the triple scattering contribution (χ_4), and all successive odd orders of scattering involving the rattling of the photoelectron between the two atoms. For n larger than 2, γ^n is the *irreducible* signal from an n-atom configuration, meaning that the lower order γ^m (with $m < n$) signals are removed. For a complete derivation of the γ^n signals, see Sec. II.C. of Ref. [21].

To make use of the n-body decomposition, the input cluster must be analyzed to extract all n-body configurations. Even in a finite cluster, there are an infinite number of n-body configurations. In practice [32], it is adequate to limit the decomposition to configurations of low order ($n \leq 4$) and within the first few coordination shells. Degeneracy – n-body configurations that produce identical signal, as from the atoms of the same species in a well ordered coordination shell – is accounted for. Non-Gaussian disorder is considered by integrating over appropriate n-body distribution functions. The EXAFS data is then fit using these γ^n signals as theoretical fitting standards modified by parameters of the coordination environment.

11.1.2 The exact curved wave theory in EXCURVE

Early work [17] provided a computationally demanding but exact, curved-wave approach to the EXAFS theory. The earliest effort at a user-oriented theory was EXCURVE. This simplified the computation of the Lee and Pendry theory such that it could be incorporated into routine analysis, but only for the single scattering contribution. Later improvements [20] extended this exact theory to low order multiple scattering. However, the approach taken by these early version of EXCURVE did not scale well in terms of computation time and so was restricted in its solution to Eq. (11.7) to single, double, and triple scattering paths.

Although less used today than the other two user-oriented theory packages, EXCURVE was central to several important developments in EXAFS. It was the first code for EXAFS analysis incorporated into professionally supported, commercial software with a sophisticated graphical interface.[1] EXCURVE was used in early discussions of constrained fitting in EXAFS [33], which is the topic of Sec. 11.2.3. It was the software used in an early efforts to corefine [34] EXAFS and diffraction data measured on the same material, which remains a thriving research area. Finally, it was the basis of a successful effort [35] to automate EXAFS analysis.

[1]Certain commercial software is identified in this chapter to foster understanding. Such identification does not imply recommendation or endorsement by the National Institute of Standards and Technology, nor does it imply that the materials or equipment identified are necessarily the best available for the purpose.

11.1.3 The path expansion in FEFF

By version 6 [22], FEFF brought several innovations to the EXAFS analysis problem, including a fast, convergent, separable representation of the photoelectron propagator. [36] This is a substantial improvement over the exact theory in EXCURVE (it was later adopted by EXCURVE) both in terms of speed of computation and by enabling consideration of multiple scattering to any order. The second was an efficient, exhaustive algorithm for the enumeration of all single and multiple scattering paths in an input cluster. [37] Even in a small cluster of atoms, the number of possible scattering paths is infinite, if all orders of scattering paths are considered. FEFF6 introduced the concept of an importance factor for each path computed as a sparse, trapezoid integration of the magnitude of the calculated, complex $\chi(k)$. In this way, paths could be assessed for spectral weight and those contributing very little to the total $\chi(k)$ could be discarded.

It is useful to understand how the path expansion relates to the n-body decomposition of GNXAS. With reference to Fig. 11.3, FEFF calculates each path (up to some order) on the right side of the equation, whereas the function calculated by GNXAS is their sum on the left side. In one way, FEFF's path expansion is less convenient as the sum of paths has far more terms than the sum of n-body configurations. However, consideration of individual paths allows for a more careful treatment of σ^2 for multiple scattering paths.

A full treatment of all aspects of FEFF's approach to the theory of EXAFS is presented in Ref. [24]. The remainder of this chapter will be written in reference to FEFF and to one specific analysis package, IFEFFIT [38], but hopefully in a way that is useful regardless of the choices of theory and analysis packages the reader makes.

11.2 Theoretical calculation of EXAFS scattering factors

Theoretical calculations of EXAFS scattering factors address most of the limitations presented by the purely empirical analysis techniques discussed above. With this theoretical tool, EXAFS can be done on meta-stable, *in situ*, or *in operando* materials or on any material otherwise unavailable as a measurement standard. Complex systems – doped, mixed phase, surface sorbed or anything else with scatterer species or distances that are not represented in readily available standards – can be analyzed. Finally, these theoretical tools provide a rigorous way of including multiple scattering contributions and higher coordination shells.

As discussed in the previous section, construction of the scattering potentials and enumeration of scattering paths are two essential components of the theoretical scattering factors used for EXAFS analysis. These calculations begin by preparing a list of Cartesian coordinates of atoms as input for the theory program. This list can come from a variety of sources, including crystallographic structure data, a large molecule structure, or the output of a first principles or molecular dynamics calculation. In any case, a list of atomic species and their Cartesian coordinates is the requisite input data. In Sec. 11.3.2, an approach is explained for using theoretical scattering factors in a case where details of the structure cannot be known beforehand.

If the input structure comes from a reliable source – that is, the distances between atoms are physically reasonable – then the MT potentials will be calculated well enough to yield a defensible EXAFS analysis. [39] Similarly, if input atoms are at nonphysical separations, the resulting calculation will be unacceptable for analysis.

A simplified method of generating theoretical scattering factors for use in first shell analysis [40] involves prompting the user for the absorber and scatterer species and their approximate separation. Using this, a rock-salt (or another similarly simple structure) configuration is constructed and used to compute the MT potentials. In Fig. 11.4, the effect of an nonphysically large MT radius is shown on the computed $\chi(k)$ for S neighbors at the Fe K edge in FeS_2. For the first coordination shell, the simplified method works well, yielding nearly identical results as a calculation made on the known crystal structure of FeS_2.

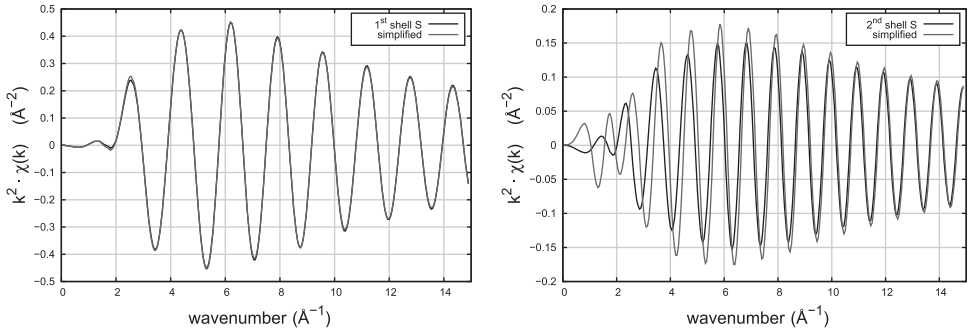

Figure 11.4 *$\chi(k)$ calculated for the first shell (left) and second shell (right) Fe-S paths in FeS_2. The black trace is $\chi(k)$ computed using the known crystal structure of FeS_2. The gray trace is $\chi(k)$ computed using the simplified method described in the text. The inter-atomic distance used in the simplified calculation on the left is the known near neighbor distance in FeS_2, while on the right the second shell distance is used. This results in nonphysical muffin tin radii and significant error in the calculated $\chi(k)$.*

The right side of Fig. 11.4 shows the second shell Fe-S path computed from the known crystal structure along with the simplified calculation using the inter-atomic distance of the second coordination shell. In that case, the simplified calculation uses a large inter-atomic distance to make the notional rock-salt structure. This yields a nonphysical MT radius and results in substantial error.

This demonstrates two important aspects of the application of theoretical scattering factors to EXAFS analysis, (1) the importance of good MT potentials with sensible radii and (2) the need for a reasonable input structure for EXAFS analysis beyond the first coordination shell.

11.2.1 The pathfinder

The next chore is to enumerate the scattering paths. An exhaustive algorithm [37] was included with FEFF6 [22]. It begins by first enumerating all single scattering (SS) paths within the input cluster. That is, it finds all paths which leave the absorber (the white atom in Fig. 11.5) and scatter only once from another atom in the cluster. Beginning with each single scattering path, every possible double scattering (DS) path is constructed by extending each single scattering path to all possible third atoms – the black atom in the middle of Fig. 11.5 – in the cluster. However, the photoelectron cannot scatter twice from the same atom, so the successive atom must be different. Each subsequent higher order of scattering is then constructed from the previous order by extending from the last atom of every path to every other atoms in cluster. In this way, an exhaustive list

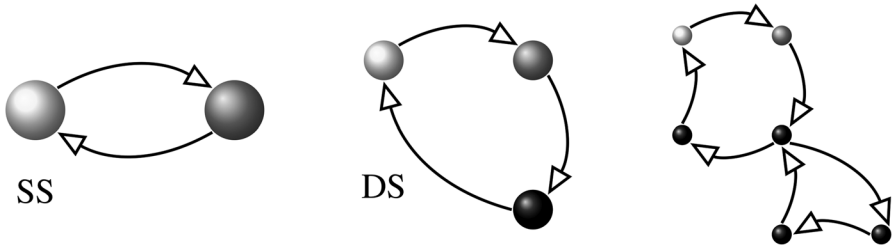

Figure 11.5 *Schematic illustrating the sequential construction of multiple scattering paths.*

of scattering paths is made. An example of a high order multiple scattering path built from the DS path is shown on the right of Fig. 11.5. For triple scattering (four-legged) paths and higher, the possibility that the photoelectron scatters from the absorber between two of its interior legs must be considered. In FEFF, this path expansion is truncated at eight legs.

The paths are sorted by increasing half-path length using a *heap*, which is a tree-like data structure [41] constructed to guarantee that the path with the shortest half-path length is always at the top of the tree. The half-path length is defined as half of the sum of the lengths of each leg. For a SS path, then, the half-path length is the atomic separation. As paths are removed from the heap, they are compared for degeneracy with all paths previously removed from the heap. An obvious example of degeneracy is two SS paths from atoms in the first coordination shell. Since these two paths would produce identical contributions to the EXAFS, they are considered degenerate. Various non-obvious sorts of degeneracy are considered, including time-reversal (scattering from the atoms in a multiple scattering path in the opposite order) or mirror symmetry about a plane in a high order path. The impact of polarization and ellipticity of the incident beam can also be considered at this stage.

With a set of MT potentials and an exhaustive list of scattering geometries, all possible contributions to the EXAFS can be computed and presented for use in analysis. For any path of any order, the atomic terms of the EXAFS equation – $F_\Gamma(k)$, the effective scattering amplitude over all atoms in the path; $\delta_\Gamma(k)$, the effective phase shift due to interaction of the photoelectron with the central atom and all scattering atoms; and $\lambda_\Gamma(k)$, the photoelectron mean free path – are computed based on the MT potentials and the scattering geometry. Here, Γ is the index counting over all paths.

This presentation of the theoretical scattering factors maps naturally onto the EXAFS equation. [16] The terms calculated by the theory program are used in the EXAFS equation, Eq. (11.1). The other terms are somehow determined as part of the analysis. All the terms in Eq. (11.1) are explained in Table 11.1. The EXAFS signal from the input cluster is then found by evaluating Eq. (11.1) for every path, the summing these contributions, as in Eq. (11.2).

Eq. (11.7) is an infinite series. In practice, however, this series is severely truncated. The half-length of the path indicates the region in R-space in which the path contributes Fourier components. Because the range over which the EXAFS data are analyzed rarely exceeds about 6 Å, paths with half-lengths much longer than 6 Å are safely neglected. Also, different paths contribute different spectral intensity. The photoelectron scattering amplitude is peaked in the forward and backward directions [17], thus paths with steep scattering angles tends to be quite small. Paths which contribute scant spectral weight can also safely be neglected. The sum in Eq. (11.2) will typically include only a few to a few dozen significant paths.

11.2.2 The fitting metric

The terms of Eq. (11.1) are evaluated and the sum, Eq. (11.2), is compared to the data. Many of the popular analysis programs which use theoretical scattering factors from FEFF employ a conventional, Levenberg-Marquardt, non-linear minimization [42]. This involves the minimization of a χ^2 fitting metric.[2] A difference function, f, between the data and calculation is computed at each data point included in the evaluation of the fit. For a fit evaluated in k-space with real-valued functions, this difference is of the form of Eq. (11.8). For a fit evaluated in the R-space, the difference function includes the real and imaginary parts of the Fourier-transformed data and calculation, as in Eq. (11.9). (The difference function for Fourier filtered data, also

[2]Unhappily, the letter χ serves two purposes in the EXAFS literature. In this chapter, the fitting metric is always squared (as in χ^2) whereas the function usually has an argument (e.g. $\chi(k)$).

complex-valued, is also of the form of Eq. (11.9), albeit with wavenumber as the abscissa.) The fitting metric is then evaluated as the sum of squares over all data points N included in the fit, Eq. (11.10).

$$f(k_i) = \chi(k_i|\mathsf{data}) - \chi(k_i|\mathsf{theory}) \tag{11.8}$$

$$f(R_i) = \mathrm{Re}\left[\tilde{\chi}(R_i|\mathsf{data}) - \tilde{\chi}(R_i|\mathsf{theory})\right] + \mathrm{Im}\left[\tilde{\chi}(R_i|\mathsf{data}) - \tilde{\chi}(R_i|\mathsf{theory})\right] \tag{11.9}$$

$$\chi^2 = \frac{N_{\mathrm{idp}}}{N}\sum_{i=1}^{N}\left(\frac{f_i}{\epsilon_i}\right)^2 \tag{11.10}$$

ϵ_i is the measurement uncertainty at data point i. N_{idp} is the information content – the number of independent points – of the data. Typically, the EXAFS data are quite over-sampled compared to the information content. N, the number of data points, is typically a few hundred while N_{idp} is around 10 or 20. The prefactor N_{idp}/N, then, scales χ^2 to the number of independent measurements in the data.

Within the context of a Levenberg-Marquardt minimization, the estimation of the size of N_{idp} is commonly taken as the Nyquist criterion [43], i.e. the bandwidth of a signal processing problem. In the context of EXAFS analysis $N_{\mathrm{idp}} \approx 2\Delta k\Delta R/\pi$, where Δk is the range over which the Fourier transform window is non-zero, and ΔR is the range over which the fit is evaluated. See Refs. [44] and [45] for discussions of statistics in EXCURVE and GNXAS.

11.2.3 Constraints on parameters of the fit

Some implementations of EXAFS analysis using FEFF consider the terms of Eq. (11.1) – N, S_0^2, σ^2, E_0, and ΔR – to be the parameters of the fit. While this may be an adequate strategy when analysis is limited to the first coordination shell, it quickly becomes untenable for larger fitting models. The number of floating parameters quickly exceeds the information content of the fit as more scattering paths are considered.

To enable both the use of theoretical scattering factors beyond the first shell and the application of rich, featureful models to the EXAFS analysis, constraints between parameters are essential. With constraints, the parameters of the EXAFS equation are *not* the parameters of the fit. Rather, they are **written in terms of** the parameters of the fit.

The simplest examples of constraints are those terms in Eq. (11.1) that relate to the central atom, S_0^2 and E_0. S_0^2 is used to approximate the attenuation of the EXAFS signal due to the incomplete overlap of wave functions of the passive electrons – all the electrons other than one excited by the incident photon – in the presence of the core-hole left behind by the photoelectron with their unperturbed wave functions [30]. This is a property of the central atom, not of a specific path. Therefore, it is often reasonable to constrain S_0^2 to be the same for each path included in the fit. This means that a single parameter is floated in the fit and its value is used for S_0^2 as Eq. (11.1) is evaluated for each path. Similarly, E_0 is a parameter that aligns the energy grid of the calculation with the energy grid of the data. Often, only one such variable parameter is required in a fit and its value is used for the evaluation of each path.

More interesting constraints are typically applied to the evaluation of ΔR and σ^2. Consider the analysis of EXAFS data measured on a simple cubic structure, say copper metal or a rock-salt structure such as FeO. For a cubic material, the lattice constant is the only structural parameter. That constant and the symmetries of the cubic space group determine the locations of all atoms. As a result, the lengths of all paths can be expressed using a volumetric lattice expansion coefficient α such that, for any path,

$$\Delta R_\Gamma = \alpha \cdot R_{0,\Gamma} \tag{11.11}$$

where $R_{0,\Gamma}$ is explained in Table 11.1. Here, α is the *parameter of the fit* and the ΔR for every path are written *in terms of* α. While this particular formulation is only valid for cubic crystals, conceptually similar

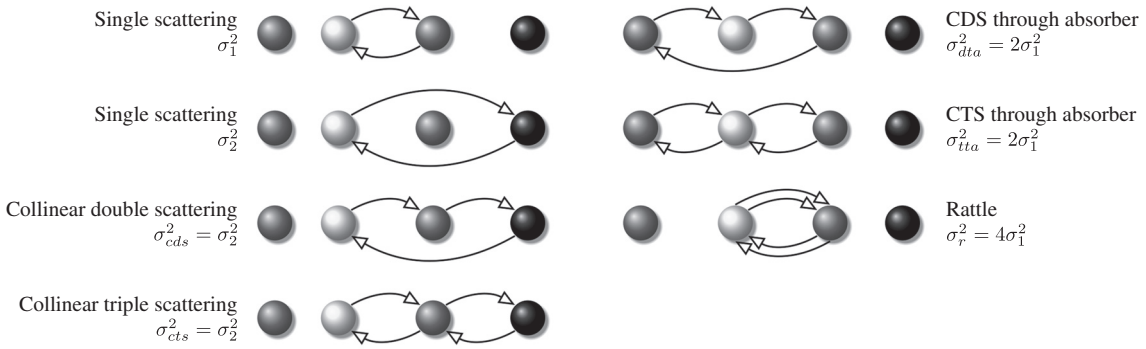

Figure 11.6 *Types of low-order collinear MS. The white ball is the absorber, the gray balls are atoms in the first coordination shell, the black ball is an atom in a more distant shell. For example, in copper metal, the black ball might be a Cu atom in the 4th shell. In the Ti K edge of cubic $EuTiO_3$, the black ball could be a Ti atom in the 3rd shell.*

constraints using more variable parameters can be applied to systems of lower symmetry. A more elaborate constraint on a ΔR parameter is shown in Sec. 11.3.1.

Constraints can be placed on σ^2 parameters. One common strategy is to treat a pair of atoms as masses bound by a quantum oscillator, thus expressing σ^2 for a path in terms of an Einstein temperature [46]. This is particularly effective for a model which considers the temperature dependence of σ^2 for a path. Another model described in that same reference relates the σ^2 values for all paths in a monoatomic crystal to its acoustic phonon spectrum. This is attractive as it allows evaluation of all σ^2 parameters in Eq. (11.1) using a single variable representing the Debye temperature of the material. Unfortunately, few EXAFS analysis problems involve monoatomic materials, limiting the utility of that approach.

The σ^2 parameters of collinear MS paths are related to the σ^2 values of geometrically related SS paths with two reasonable assumptions [47], the thermal motion in the perpendicular direction is small compared to the separation between the atoms and the thermal motions of the atoms are uncorrelated. Given those assumptions, the relations between the σ^2 parameters given in Fig. 11.6 are obtained, allowing parameterization of *all* of these paths using only two variable σ^2 parameters in the fit. In certain situations, it is possible to relate the σ^2 of non-collinear MS paths to the σ^2 of the SS paths made up of legs in the MS path. In Ref. [32], a formula is given as Equation 13 for a triangular configuration of Ge atoms in crystalline germanium.

The constraints discussed in the last few paragraphs represent ways of encoding *prior knowledge* into a fit. Consider the example of representing all the ΔR parameters using a single lattice expansion parameter. In this case, our prior knowledge is that the material is cubic and the lengths of the paths must be constrained by cubic symmetry. Acknowledging this by using constraints in the fit serves to reduce the number of fitting parameters which must be determined by the fit and, hopefully, to make the fit more statistically robust.

11.2.4 Fitting statistics

One reasonable definition [38] of an R-factor for EXAFS is

$$\mathcal{R} = \frac{\sum_{i=1}^{N} \left[f(R_i)\right]^2}{\sum_{i=1}^{N} \left(\left[\mathrm{Re}\left(\tilde{\chi}(R_i|\mathsf{data})\right)\right]^2 + \left[\mathrm{Im}\left(\tilde{\chi}(R_i|\mathsf{data})\right)\right]^2 \right)} \tag{11.12}$$

where $f(R_i)$ is from Eq. (11.9) and $\mathcal{R}$ is evaluated over all data points included in the fit. ($\mathcal{R}$ evaluated in k-space takes the same form, except that the denominator is the sum of squares of the real-valued $\chi(k)$ function.) In this form, $\mathcal{R}$ is interpreted as a percentage misfit or, equivalently, as a numerical evaluation of how closely the fitted function overplots the data. As such it is a useful metric for judging misfit, but not fit quality. One can imagine a scenario in which $\mathcal{R}$ is small, but the fitted values of one or more fitting parameters are physically indefensible.

The *reduced chi-square* is a metric which weights the closeness of the fitted function to the data by the unused information content:

$$\chi^2_\nu = \frac{\chi^2}{\nu} \quad \text{where} \quad \nu = N_{\text{idp}} - N_{\text{var}}. \tag{11.13}$$

N_{var} is the number of parameters evaluated in the fit, thus ν is the unused portion of the information content. The value of χ^2_ν is that it allows comparison of fits using different fitting models. Consider a fit to Fe K edge data measured on Fe_2O_3, hematite. This is a rhombohedral crystal [48] in which the first coordination shell is split into two distances, 1.946 Å and 2.116 Å, each populated by 3 oxygen atoms. One might wish to know whether σ^2 can be measured independently for these two oxygen scatterers given the quality of the data. χ^2_ν offers a way of answering that question. Adding a second σ^2 parameter increases N_{var} and reduces ν. If χ^2_ν decreases sufficiently when that second parameter is added to the fit, then one might have confidence that the two σ^2 parameters can be measured. On the other hand, if χ^2_ν changes little or increases upon adding the second σ^2 parameter, then the data cannot support their independent measurement.

Formally, χ^2_ν provides an absolute metric [42] of goodness of fit. If $\chi^2_\nu \approx 1$, then the data are consistent with the fitting model. Typically in EXAFS, χ^2_ν is rarely near 1. Consider the fit to the first shell of room temperature, metallic gold shown in Fig. 11.7. Theoretical scattering factors using FEFF was computed using face-centered cubic gold with a lattice constant of 4.08 Å. The Fourier transform and fit ranges are given by the vertical, dotted lines. With N fixed to 12, this fit resulted in $S_0^2 = 0.85(4)$, $E_0 = 5.56(31)$ eV, $\Delta R = -0.023(3)$ Å, $\sigma^2 = 0.00824(34)$ Å^2, and $\mathcal{R} = 0.0070$. This is unambiguously an acceptable fit – the misfit is well below 1% and the values of all four fitting parameters are physically defensible and with small uncertainties. However, $\chi^2_\nu = 754.0$, supposedly indicating an extremely poor fit. How can this be?

The resolution to this apparent incongruity is the evaluation of ϵ, the measurement uncertainty, in Eq. (11.10). It is, at best, extremely difficult to evaluate ϵ well. In most EXAFS measurements, it is not measured at all. (Ref. [49] is a rare and welcome exception.) One way of approximating ϵ is to presume that no structural information persists above 15 Å in $\tilde{\chi}(R)$. The average value of $|\tilde{\chi}(R)|$ in the range from 15 Å to 25 Å is computed and used [38] for each ϵ_i in Eq. (11.10).

The tacit assumption behind this evaluation of ϵ is that the noise is dominated by statistical variation. This is a poor assumption when a synchrotron source is used for the EXAFS measurement. Except for the most dilute samples measured in fluorescence, the flux incident upon the experiment, even from a second generation source, is so high that statistical variation is typically small compared to instrumental sources of uncertainty and to error in the theoretical scattering factors. When the evaluation of ϵ is too small, χ^2_ν is too large, even for an obviously good fit. With ambiguity in ϵ, χ^2_ν is not a useful parameter for evaluating the goodness of a *single* fit.

Still, χ^2_ν is an essential statistical parameter. Examination of χ^2_ν allows the EXAFS analyst to determine whether a fit is improved by adding additional paths or variables. When χ^2_ν is significantly reduced by the addition or removal of a parameter or a path, the resulting fit can, with confidence, be said to have improved.

The question remains of how to determine whether a particular fit is, in fact, a good fit. The resolution is to consider whether the results of an analysis are *defensible*. While it is certainly true that a defensible fit will have small values for $\mathcal{R}$ and χ^2_ν, examination of the fitted values for the variable parameters and of the evaluations of the parameters of Eq. (11.1) is essential. Parameter values must be sane. Some rules of thumb

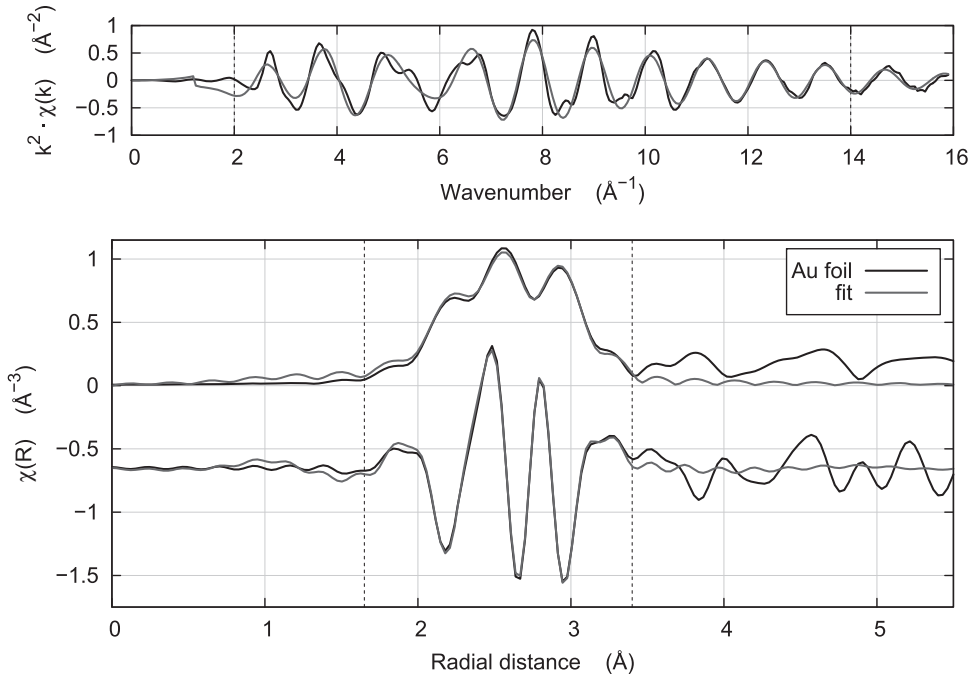

Figure 11.7 *The result of a simple fit to the first coordination shell in metallic gold. The data (black) are overplotted with the best fit function (gray) as* $\chi(k)$*,* $|\tilde{\chi}(R)|$*, and* $\mathrm{Re}[\tilde{\chi}(R)]$.

include that S_0^2 [50, 30] not be much smaller than 0.7 or much larger than 1.0, that ΔR values not result in nonphysical distances between atoms, that σ^2 – the mean *square* variation in distance – not be negative, and that E_0 shifts should not be so large [51] that the fit finds a false minimum. While a particular sophisticated fitting model might parameterize Eq. (11.1) in a way that does not observe these rules of thumb, it is certainly true that a defensible fit results in defensible values for all fitting parameters.

Error bars The algorithm for finding the minimum of the fit also yields a matrix [42] whose diagonal elements are the error margins for each variable parameter and whose off-diagonal elements are the correlations between the variables. When ϵ is too small, χ_ν^2 is too large and the diagonal elements of the matrix are too small and do not correctly represent the level of uncertainty in the variable parameters. To correct for this, the diagonal elements are scaled by $\sqrt{\chi_\nu^2}$, resulting in error margins that would be correct were ϵ evaluated correctly *and* under the assumption that the fit is a good fit. Therefore, if you consider a fit to be defensible, the error margins scaled in this way are defensible 1σ uncertainties.

Correlations Certain correlations between parameters are unavoidable. Even in the excellent fit to Au foil shown in Fig. 11.7, the S_0^2 and σ^2 parameters are over 80% correlated, meaning that a statistically equivalent fit can be recovered by changing one parameter within its error margin so long as the correlated parameter changes by 80% of that amount. Similarly, the E_0 and ΔR parameters are nearly 70% correlated. While low correlations between parameters is desirable as it indicates robustness of the parameterization, it is common for parameters effecting the amplitude (or the phase) of Eq. (11.1) to be highly correlated.

11.2.5 Extending the evaluation of χ^2

Multiple FEFF calculations Many EXAFS analysis problems cannot be solved by a single calculation of the theory program. Examples include mixed-phase systems for which each phase contains the absorbing atom, crystal systems for which the absorber sits on more than one crystallographic site, metalloproteins with multiple active sites, or any other situation for which the absorbing atom exists in two or more distinct coordination environments.

In any such case, the general form of the solution is the same. The theory program is run for each distinct coordination environment. Paths are used from each such calculation to model that component of the measured data. The summation in Eq. (11.2) then includes paths from two or more calculations. An example is discussed in Sec. 11.3.2.

Multiple data sets A sample might be measured at several temperatures or pressures or at the edge of two or more elements. This suggests the prospect of corefinement of data. As a practical matter, corefinement of multiple data sets is a simple modification of Eq. (11.10). Eqs. (11.1) and (11.2) are evaluated for the paths used to model each data set, then Eq. (11.10) is evaluated with an additional summation over all data sets.

The great advantage of a multiple data set fit is that it multiplies the information available to the fit. N_{idp} is evaluated for each data set and summed. A corefinement becomes attractive when an aspect of the fitting model either is independent of the extrinsic parameter or can be modeled in terms of the extrinsic parameter. For example, in a temperature series for which the data have been carefully aligned onto a common energy axis, a single E_0 parameter (see Table 11.1) can be used for each data set. In a temperature series, σ^2 for a path might be related at all temperatures to a single Einstein temperature [46]. Likewise, ΔR might be related to a linear expansion coefficient. In each case, the information content of the fit is increased without similarly increasing the number of variable parameters.

EXAFS data from multiple edges in a material present interesting possibilities for constraints in the context of a multiple data set fit. Consider $EuTiO_3$, a cubic perovskite. The data measured at the Eu L_{III} and Ti K edges must see the same lattice constant. The second coordination shell of each edge contains the other metal as a scatterer. σ^2 for that path must be the same when observed with either metal as the absorber. The use of multiple data set in a problem with data measured at multiple edges is discussed in Sec. 11.3.3.

Multiple k-weights In EXAFS analysis, it is common to perform the analysis on k^n-weighted data, where typically $n \in [1, 2, 3]$, but could be a non-integer value as well. That is, the $\chi(k)$ function is multiplied by some exponent of k before further data analysis. For example, in Fig. 11.7, the $\chi(k)$ data are displayed with $n = 2$. This serves to scale the oscillations such that they are of about the same size over the entire energy range of the data. The Fourier transform was then performed on the k^2-weighted data.

Weighting the data by different exponents of k can serve a numerical purpose in the analysis by changing the relative importance of different energy regions in the evaluation of the fit. Because σ^2 is multiplied by k^2 in Eq. (11.1), a misfit in the value of σ^2 will have more profound impact on the evaluation of χ^2 at the high-k end of the data. Using a larger n, therefore, will increase the sensitivity of the evaluation of χ^2 to a misfit in σ^2. In similar fashion, the sensitivity of the evaluation of χ^2 to a misfit in E_0 is greater at low k (see the expression of E_0 in Table 11.1). Using a smaller n will, therefore, increase the sensitivity of the evaluation of χ^2 to a misfit in E_0.

Eq. (11.10) is extended such that χ^2 is evaluated for each value of k^n-weighting included in the model. The sum of these χ^2 values is the quantity minimized in the fit. This provides an effective compromise between the merits of the different k-weighting options, enhancing the sensitivity of the evaluation of χ^2 over the entire k range.

11.2.6 Other analytic methods

The discussion in this chapter covers current practice common by many of the most widely used EXAFS data analysis packages. In no sense can this the discussion in this chapter be considered "modern" in 2014, the year that this chapter was written. Most of the theory of EXAFS was in place by the mid 1990s. The statistical formalism described here was developed decades earlier. Aside from the graphical user interfaces employed by some EXAFS analysis packages, most of the EXAFS software of today could have been written in 1995. That is not a criticism – concepts that are useful and productive tend to age gracefully.

That said, EXAFS researchers have explored many new ideas in the last twenty years. Two prominent areas that merit attention are Bayesian statistical analysis and the use of the wavelet transformation. While full treatment of these topics is beyond the scope of this chapter, overviews are presented here.

Bayesian statistics There are a number of problematic aspects of the statistical discussion in the preceding pages. The difficulty determining an appropriate estimate of ϵ leads to several ambiguities in the analysis, including the absolute determination of goodness of fit and the scaling of error bars. In multiple data set or multiple k-weight fits, no explanation was given for how to weight the relative importance of the different components of the evaluation of χ^2. Even the determination of the number of independent points, given after Eq. (11.10), results from an analogy with the theory of signal processing that is unlikely to hold true for a typical EXAFS analysis problem. In short, the conventional formulation of the EXAFS χ^2 minimization problem is usually ill-posed. Despite this problem, the application of the simple statistical model presented in this chapter has proven successful, albeit only when approached conservatively and skeptically.

This approach can be improved upon. Bayesian inference provides a rational system for evaluating assumptions made about a body of data and updating those assumptions on the basis of the measured data. Refs. [52, 53] demonstrate an approach to assessing the value of prior knowledge and the reliability of measured data. By this algorithm, the ill-posed problem is reduced to a series of well-posed, linear equations. Then a series of non-linear equations are evaluated iteratively to determine the relationship of the prior knowledge and the data to the confidence in the result.

This approach contributes a significant solution to each of the shortcomings of the conventional approach. The problems of evaluating measurement uncertainty, confidence in prior knowledge, and confidence in different portions of the data ensemble are treated formally. This Bayesian approach even provides a rigorous way to evaluate the true information content of the data. The treatment presented in Ref. [52, 53] is the most thorough discussion of Bayesian methods as applied to EXAFS, but its demonstration was limited to rather simple examples of measured and synthetic data. Other authors have applied Bayesian methods to more realistic research problems, see, for example, Refs. [54] and [55]. As a practical matter, prior knowledge is always used in some sense in the formulation of fitting models for use in EXAFS analysis, as is demonstrated by the examples in Sec. 11.3.

Wavelet transforms The basis used in a Fourier transform – an integration of $\chi(k)$ over the exponential e^{ikR} – is delocalized in k space and completely localized in R space. In EXAFS measurement, however, $\chi_\Gamma(k)$ is not infinite. Since the measured $\chi(k)$ is typically defined beginning around 3 Å^{-1} and extending for only about 5 Å^{-1} to 15 Å^{-1}, the $\tilde{\chi}(R)$ signal will be quite broad even before consideration of the σ^2 term in Eq. (11.1). The wavelet transform offers a tool for distinguishing overlapping scatterers by use of basis functions that are partially localized in both k and R. [56, 57] In a situation where two overlapping scatterers are considerably different in mass, their scattering functions will be peaked in amplitude in different regions of k space. As a general rule, light elements are peaked at low k, while heavier elements have signals that extend to much higher k. Very heavy elements show a Ramsauer-Townsend [58] effect in their scattering amplitudes, adding additional structure to $\chi_\Gamma(k)$ in some k range. If a basis can be found with components localized in k space in a way that emphasizes one kind of scatterer over another, then the wavelet transform

might provide a much needed sensitivity in the case of scatterers at similar distances. In most applications to EXAFS analysis, Morlet wavelets [59] are used. One particularly interesting implementation of the wavelet transform [60] uses scattering functions from FEFF to define wavelets which are specialized for application to EXAFS analysis.

The use of multiple k-weights discussed in Sec. 11.2.5 bears a certain similarity to the use of wavelet transforms. By including terms in the evaluation of χ^2 with different sensitivities to different regions of k space, the fitting model is often able to resolve ambiguities introduced by different scattering species at similar distances. Well-chosen wavelets, particularly those based on scattering functions from EXAFS theory, might be a more refined tool for resolving these ambiguities in a data analysis.

11.3 Practical examples of EXAFS analysis

This section further explores the notion that the parameters of the EXAFS equation, Eq. (11.1), are not the parameters of the fit but are, instead, written in terms of the parameters of the fit. This use of prior knowledge to create rich, sophisticated fitting models is central to the practice of EXAFS analysis.

11.3.1 Geometric constraints on bond lengths

In Ref. [61], EXAFS measurements were made on an artificial DNA construct proposed as a sensor for mercury in solution. The DNA construct is specifically engineered to be selective for a particular metal. The binding of the metal to the DNA results in the activation of a phosphor, which provides the optical signal making this a metal sensor. The purpose of the EXAFS measure was to identify the bonding environment of the mercury atom to the DNA sensor. Earlier work by nuclear magnetic resonance suggested that the Hg atom replaces the weak hydrogen bond between a thymidine-thymidine mispair.

The analysis started from the known structure [62] of the nucleotides. To avoid bias in the result of the analysis, the possibility of the Hg atom bonding to any position on any of the four nucleotides was considered. Several such positions are shown for thymidine in Fig. 11.8. The Hg might bond to a corner of a nitrogenous base, to a corner of a sugar (marked as $\overline{\text{Hg}}$), or even bound to the nucleotide via a monodentate bridge (two examples are marked as $\widetilde{\text{Hg}}$). Obviously, these options are not equally likely from a chemical perspective, but each can be tested against the EXAFS data.

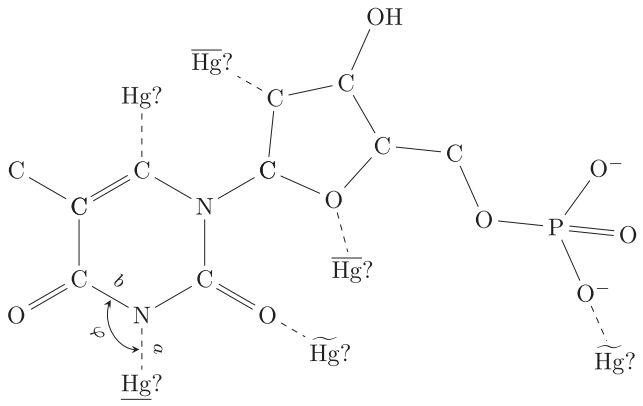

Figure 11.8 *Schematic of some conceivable ways that Hg might bond to thymidine.*

The data, seen in Ref. [61], define the approximate distance of the Hg atom from its nearest neighbor, ∼2.04 Å. Input for FEFF was created using the nucleotide structure and with the Hg absorber placed at that distance in each of the many possible locations. The data itself eliminated several possible absorber environments. Of the three kinds of locations shown in Fig. 11.8, only a position close to the corner of a six-member ring provided second shell scatterers at a distance that is consistent with the data. The $\overline{\text{Hg}}$ and $\widetilde{\text{Hg}}$ locations were therefore eliminated from consideration.

Because of the limited data quality, the information content of the data was quite small. This required a highly constrained model. The distance from the Hg atom to the near neighbor N or C atom, a, was a variable parameter. The nitrogenous base was presumed to be rigid such that the change in N–C or C–C distance could be neglected. Consequently, the distance from the Hg absorber to scatterers in the second shell was constrained by a standard trigonometric relation:

$$D(\text{Hg–2NN}) = \frac{(a-b)\cos(\varphi/2)}{\cos(\beta)} \quad \text{where} \quad \tan(\beta) = \frac{a+b}{a-b}\tan(\varphi/2) \tag{11.14}$$

and a, b, and φ are all indicated in Fig. 11.8. In the fit, b was fixed to its nominal value while a was a variable. Thus, the distances to atoms in both the first and second coordination shells were evaluated with a single variable. This constraint enabled a fitting model which effectively used the limited information content of the data. In the end, the data supported the Hg atom being bound to thymidine at the location marked as $\underline{\text{Hg}}$ in Fig. 11.8.

11.3.2 Constraints on the coordination environment

In Ref. [63], EXAFS measurements were made on suspensions of the bacterium *B. subtilis* which were allowed to come to equilibrium with aqueous uranyl solutions. The point of the experiment was to understand how the uranyl ions bind with the biomass in the solution. The authors found that the uranyl has a strong affinity for phosphoryl ligands at very low pH with an increasing affinity for carbonyl ligands as the pH increased.

In this analysis problem, the uranyl ions are in equilibrium with an uncharacterized biomass. There is no obvious initial structure for this system, yet theoretical scattering factors from FEFF was used effectively in the analysis. To start, the authors recognized that there are only a few plausible coordination environments for the uranyl ion, all of which are shown schematically in Fig. 11.9. In short, the uranyl can be bound to a phosphoryl ligand via a monodentate bridge, to a carbonyl ligand via a bidentate bridge, or to a hydroxyl ligand (represented by the dangling equatorial oxygen atoms). The oxygen atom forming the phosphoryl bridge is at a distance of about 2.35 Å, while the two oxygen atoms forming the carbonyl bridge are at a distance of about 2.42 Å. The U–O distance for the hydroxyl ligand is also about 2.42 Å.

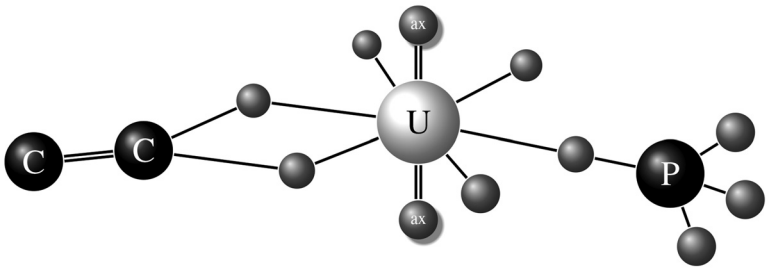

Figure 11.9 *Schematic of the possible uranyl bonding environments. The uranyl ion consists of 5 or 6 equatorial oxygen atoms and two very short axial oxygenyl ligands.*

To generate theoretical standards for the fit, FEFF was run on two crystalline materials, triuranyl diphosphate tetrahydrate [64] and sodium uranyl triacetate [65]. The authors certainly did not expect to find either of those minerals in their sample. However, the positions of the uranium, oxygen, and phosphorous atoms from the first mineral are an effective representation of the similar configurational unit found in the biomass sample. Similarly, the positions of the uranium, oxygen, and carbon atoms in the second mineral effectively represent the carbonyl structure in the biomass sample.

The fitting model described in Ref. [63] uses constraints involving distances and coordination numbers. The number of oxygen scatterers at the short distance, ∼2.35 Å, must equal the number of phosphorus scatterers. Likewise, the number of carbon scatterers can be no more than half the number of oxygen scatterers at the ∼2.42 Å distance. Other constraints were considered in the fit. There are significant multiple scattering paths involving the axial oxygen atoms or the nearly collinear U–O–P configuration. The σ^2 parameters for those paths used the constraints given in Fig. 11.6.

Using theoretical scattering factors calculated on closely related structures and employing constraints that encapsulate essential features of the coordination environment, the authors were able to understand the pH dependence of the bonding of the uranyl ion to biomass.

11.3.3 Constraints and multiple data set analysis

Nanoscale manganese zinc ferrite samples are studied by EXAFS in Ref. [66]. These materials present an interesting structural challenge due to the distribution of the three transition metals over the tetrahedral and octahedral sites of the spinel structure. Because the x-ray scattering strength of the three metals are so similar, determination of site occupancy using diffraction would require resonant techniques. However, because the particles are so small, the peak broadening limits the information that can be extracted from a conventional x-ray diffraction measurement. To address the problem of site occupancy, the authors measured EXAFS on all three edges and performed multiple data set fitting to best use the data ensemble. With the three data sets all providing information to the fit, a sophisticated structural model could be applied. In short, the two coordination environments, shown schematically in Fig. 11.10, populate the spinel unit cell. The three metal atoms are distributed among these two kinds of sites. Because the number of and distance to the neighboring oxygen atoms is different in these two coordination environment, the EXAFS data at the three edges were used to determine site occupancy.

Section IV.B of that paper enumerates the list of constraints applied to the fitting model. Along with assumptions of phase and valence purity and constraints on σ^2 for multiple scattering contributions as in Fig. 11.6, several interesting constraints among the data sets were applied. Distance self-consistency required that a metal-metal distance be the same regardless of which metal is the absorber. Thus a single variable ΔR parameter was used for corresponding metal-metal paths in different data sets. Total metal stoichiometries were determined independently by inductively coupled plasma measurements and reported in the paper. These stoichiometries were used to constrain the site occupancies. For example, if the numbers of zinc and manganese scatterers on a site were used as variable parameters in the fit, the number of iron scatterers was computed from those variables and the total stoichiometries.

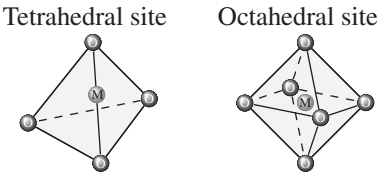

Figure 11.10 *Schematic of the two coordination environments in the inverse spinel structure.*

Several aspects of Ref. [66] make it so instructive. It demonstrates how corefinement of an ensemble of related data allows determination of structures more accurately and with greater precision than independent refinement of the data sets. It explains with clarity the purpose and application of the constraints used in the fitting model and their relation to prior knowledge, such as the independently measured stoichiometries. Throughout the paper, the authors discuss how each constraint was tested with respect to the statistical quality.

11.4 Conclusion

Of the three user-oriented theory packages discussed in Sec. 11.1, FEFF has seen the widest adoption. GNXAS continues to be popular, with dozens of citations each year, but has never been as widely used as FEFF. The use of EXCURVE seems to have diminished in recent years. Given that all three packages were successful in bringing real-space, multiple-scattering theory to bear on the EXAFS analysis problem in a user-oriented manner, what accounts for their differences in popularity and deployment?

Early in its life, EXCURVE was licensed to a company whose product was a materials measurement studio, a common framework for managing calculation and data analysis relevant to a wide variety of materials measurements. EXCURVE was its XAS component. In many ways, this was a canny arrangement by the people who developed EXCURVE. The licensee took on the difficult chores of distribution, support, and integration into a graphical work environment. For the end user, however, the cost of the software product was quite high. While development continued on a less restricted branch – EXCURV98 became DL_EXCURV [67], upon which ABRA [35] was based – FEFF's wider success is attributable in part to a lower fee for entry and less restrictive end-user licensing terms.

GNXAS presents a different story. It has always been free of cost, requiring only that its use be registered with its developers. While a redistributable, free-of-cost version of FEFF6 suitable for EXAFS analysis has been available since 2002, later versions of FEFF have always come with a licensing fee. Calculation of theoretical scattering factors and analysis are tightly integrated in GNXAS, coming in a single package from a single group of developers. In contrast FEFF is only a theory program. It encapsulates its output in a way that can be incorporated into an independent data analysis program. At this time, there are nearly a dozen such efforts actively maintained by groups with no direct connection to the FEFF project. Encouraging third party development has allowed a thriving ecosystem to evolve around FEFF.

References

[1] Beeby, J.L. (1964) The electronic structure of disordered systems. *Proc. Royal Soc. (London)*, **A279**, 82–97.
[2] Beeby, J.L. (1967) The density of electronsina perfector imperfect lattice. *Proc. Royal Soc. (London)*, **A302**, 113–136.
[3] Ankudinov, A.L., Ravel, B., Rehr, J.J. and Conradson, S.D. (1998) Real-space multiple-scattering calculation and interpretation of x-ray-absorption near-edge structure. *Phys Rev B.*, **58**, 7565–7576.
[4] Mirsky, L. (1963) *An Introduction to Linear Algebra*. Dover Books, New York.
[5] Filipponi, A. (1991) Continued fraction expansion for the X-ray absorption cross section. *J. Phys.-Condes. Matter*, **3**, 6489.
[6] Newville, M., Līviņš, P., Yacoby, Y. *et al*. (1993) Near-edge x-ray-absorption fine structure of Pb: a comparison of theory and experiment. *Phys Rev B.*, **47**, 14126–14131.
[7] Bridges, F., Booth, C.H., and Li, G.G. (1995) An iterative approach to "atomic background" removal in XAFS data analysis. *Physica B*, **208**, 121–124.
[8] Hu, T.D., Xie, Y.N., Jin, Y.L., and Liu, T. (1997) A new method for extracting x-ray absorption fine structure and the atomic background from an x-ray absorption spectrum. *J. Phys.-Condes. Matter*, **9**, 5507.
[9] Kuzmin, A. (1995) EDA: EXAFS data analysis software package. *Physica B*, **208**, 175–176.

[10] Klementev, K.V. (2001) Extraction of the fine structure from x-ray absorption spectra. *J. Phys. D-Appl. Phys.*, **34**, 209.

[11] Sayers, D.E., Stern, E.A., and Lytle, F.W. (1971) New technique for investigating noncrystalline structures: Fourier analysis of the extended x-ray-absorption fine structure. *Phys Rev Lett*, **27**, 1204–1207.

[12] Lytle, F.W., Sayers, D.E., and Stern, E.A. (1975) Extended x-ray-absorption fine-structure technique. II. Experimental practice and selected results. *Phys Rev B*, **11**, 4825–4835.

[13] Woicik, J.C., Gupta, J.A., and Crozier, D.S.P.W.E. (1998) Bond-length strain in buried $Ga_{1-x}In_xAs$ thin-alloy films grown coherently on InP (001). *Appl. Phys. Lett.*, **73**, 1269.

[14] Bunker, G. (1983) Application of the ratio method of EXAFS analysis to disordered systems. *Nucl. Instrum. Methods Phys. Res.*, **207**, 437–444.

[15] Stern, E.A., Ma, Y., Hanske-Petitpierre, O. and Bouldin, C.E. (1992) Radial distribution function in x-ray-absorption fine structure. *Phys Rev B*, **46**, 687–694.

[16] Stern, E.A. (1974) Theory of the extended x-ray-absorption fine structure. *Phys Rev B*, **10**, 3027–3037.

[17] Lee, P.A. and Pendry, J.B. (1975) Theory of the extended x-ray absorption fine structure. *Phys Rev B*, **11**, 2795–2811.

[18] Ashley, C.A. and Doniach, S. (1975) Theory of extended x-ray absorption edge fine structure (EXAFS) in crystalline solids. *Phys Rev B*, **11**, 1279–1288.

[19] Newville, M. (2014) Fundamentals of XAFS. *Rev. Mineral. Geochem.*, **78**, 33–74.

[20] Gurman, S.J., Binsted, N., and Ross, I. (1986) A rapid, exact, curved-wave theory for EXAFS calculations. II. The multiple-scattering contributions. *J. Phys. C: Solid State Phys.*, **19**, 1845–1861.

[21] Filipponi, A., Di-Cicco, A., and Natoli, C.R. (1995) X-ray absorption spectroscopy and nbody distribution functions in condensed matter. *I. Theory. Phys Rev B*, **52**, 15122–15135.

[22] Zabinsky, S.I., Rehr, J.J., Ankudinov, A. *et al*. (1995) Multiple-scattering calculations of x-ray-absorption spectra. *Phys Rev B*, **52**, 2995–3009.

[23] Slater, J.C. (1937) Wave functions in a periodic potential. *Phys Rev*, **51**, 846–851.

[24] Rehr, J.J. and Albers, R.C. (2000) Theoretical approaches to x-ray absorption fine structure. *Rev. Mod. Phys.*, **72**, 621.

[25] Norman, J.G. (1976) Non-empirical versus empirical choices for overlapping-sphere radii ratios in SCF-Xα-SW calculations on ClO_4 -and SiO_2. *Mol. Phys.*, **31**, 1191–1198.

[26] Joly, Y. (2001) X-ray absorption near-edge structure calculations beyond the muffin-tin approximation. *Phys Rev B.*, **63**, 125120.

[27] Rehr, J.J., Kas, J.J., Sorini, Prange, M.P., *et al*. (2009) Ab initio theory and calculations of X-ray spectra. *C. R. Phys.*, **10**, 548–559.

[28] Pauli, M.D. (1999) Constructing the muffin-tin potential. Online (http: //hermes.phys.uwm.edu/projects/elecstruct/mufpot/MP/MP.Theory4.html), accessed 18 February, 2014.

[29] Lee, P.A., and Beni, G. (1977) New method for the calculation of atomic phase shifts: application to extended x-ray absorption fine structure (EXAFS) in molecules and crystals. *Phys Rev B.* Mar, **15**, 2862–2883.

[30] Rehr, J.J., Stern, E.A., Martin, R.L., and Davidson, E.R. (1978) Extended x-ray-absorption fine-structure amplitudes: wave-function relaxation and chemical effects. *Phys Rev B*, **17**, 560–565.

[31] Lloyd, P. and Smith, O.V. (1972) Multiple scattering theory in condensed materials. *Adv. Phys.*, **21**, 69–142.

[32] Filipponi, A. and Cicco, A.D. (1995) X-ray absorption spectroscopy and n-body distribution functions in condensed matter. II. Data analysis and applications. *Phys Rev B*, **52**, 15135–15149.

[33] Binsted, N., Strange, R.W., and Hasnain, S.S. (1992) Constrained and restrained refinement in EXAFS data analysis with curved wave theory. *Biochemistry*, **31**, 12117–12125.

[34] Binsted, N., Pack, M.J., Weller, M.T., and Evans, J. (1996) Combined EXAFS and Powder Diffraction Analysis. *J. Am. Chem. Soc.*, **118**, 10200–10210.

[35] Wellenreuther, G., Parthasarathy, V., and Meyer-Klaucke, W. (2009) Towards a black-box for biological EXAFS data analysis. II. Automatic BioXAS Refinement and Analysis (ABRA). *J. Synchrot. Radiat.*, **17**, 25–35.

[36] Mustre de Leon, J., Rehr, J.J., Zabinsky, S.I., and Albers, R.C. (1991) Ab initio curved-wave x-ray absorption fine structure. *Phys Rev B.*, **44**, 4146–4156.

[37] Rehr, J.J., Albers, R.C., and Zabinsky, S.I. (1992) High-order multiple-scattering calculations of x-ray absorption fine structure. *Phys Rev Lett.* Dec, **69**, 3397–3400.

[38] Newville, M. (2001) IFEFFIT: interactive XAFS analysis and FEFF fitting. *J. Synchrot. Radiat.*, **8**, 322–324.

[39] Burattini, E., D'Angelo, P., Cicco, A.D., *et al*. (1993) Multiple scattering x-ray absorption analysis of simple brominated hydrocarbon molecules. *J. Chem. Phys.*, **97**, 5486–5494.

[40] Webb, S. (2012) SIXPACK: Sam's Interface for XAS Package, Online (http: //home.comcast.net/∼sam webb/sixpack.html) accessed 18 February, 2014.

[41] Cormen, T.H., Leiserson, C.E., Rivest, R.L., and Stein, C. (2009) *Introduction to Algorithms*. 3rd edition. The MIT Press, Cambridge, MA.

[42] Bevington, P. and Robinson, D.K. (2002) *Data Reduction and Error Analysis for the Physical Sciences*. 3rd edition. McGraw-Hill, New York.

[43] Brillouin, L. (1962) *Science and Information Theory*. Academic Press, New York.

[44] Joyner, R.W., Martin, K.J., and Meehan, P. (1987) Some applications of statistical tests in analysis of EXAFS and SEXAFS data. *J. Phys. C: Solid State Phys.*, **20**, 4005–4012.

[45] Filipponi, A. (1995) Statistical errors in X-ray absorption fine-structure data analysis. *J. Phys.-Condes. Matter*, **7**, 9343–9356.

[46] Sevillano, E., Meuth, H. and Rehr, J.J. (1979) Extended x-ray absorption fine structure Debye-Waller factors. I. Monatomic crystals. *Phys Rev B*, **20**, 4908–4911.

[47] Hudson, E.E., Allen, P.G., Terminello, L.J. *et al*. (1996) Polarized x-ray absorption spectroscopy of the uranyl ion: comparison of experiment and theory. *Phys Rev B*, **54**, 156–165.

[48] Blake, R.L., Hessevick, R.E., Zoltai, T., and Finger, L.W. (1966) Refinement of the hematite structure. *Am. Miner.*, **51**, 123–129.

[49] Chantler, C.T., Barnea, Z., C.Q. Tran, N.A.R., and de Jonge, M.D. (2012) A step toward standardization: development of accurate measurements of X-ray absorption and fluorescence. *J. Synchrot. Radiat.*, **19**, 851–862.

[50] Li, G.G., Bridges, F., and Booth, C.H. (1995) X-ray-absorption fine-structure standards: A comparison of experiment and theory. *Phys Rev B*, **52**, 6332–6348.

[51] Michalowicz, A. and Vlaic, G. (1998) Multiple solutions in data fitting: a trap in EXAFS structural analysis and some ideas to avoid it. *J. Synchrot. Radiat.*, **5**, 1317–1320.

[52] Krappe, H.J. and Rossner, H.H. (2000) Error analysis of XAFS measurements. *Phys Rev B*, **61**, 6596–6610.

[53] Krappe, H.J. and Rossner, H.H. (2002) Bayes-Turchin approach to x-ray absorption fine structure data analysis. *Phys Rev B*, **66**, 184303.

[54] Zschech, E., Blau, W., Fjodorov, V.K., and Sheromov, M.A. (1989) EXAFS investigation of $Fe_{1-x}B_x$ amorphous alloys. nuclear instruments and methods, *Nucl. Instrum. Methods Phys. Res. A*, **282**, 586–589.

[55] Sakamaki, M., Konishi, T., Fujikawa, T. *et al*. (2009) Correlation of magnetism and structure for ultra thin Au/Co/Au films: evidence for magnetoelastic effects. *J. Phys.: Conf. Series*, **190**, 012113.

[56] Muñoz, M., Argoul, P., and Farges, F. (2003) Continuous Cauchy wavelet transform analyses of EXAFS spectra: a qualitative approach. *Am. Miner.*, **88**, 694–700.

[57] Timoshenko, J. and Kuzmin, A. (2009) Wavelet data analysis of EXAFS spectra. *Comput. Phys. Commun.*, **180**, 920–925.

[58] McKale, A.G., Veal, B.W., Paulikas, A.P. *et al*. (1988) Generalized Ramsauer Townsend effect in extended x-ray-absorption fine structure. *Phys Rev B*, **38**, 10919–10921.

[59] Morlet, J., Arens, G., Fourgeau, E., and Glard, D. (1982) Wave propagation and sampling theory Part I: Complex signal and scattering in multi layered media. *Geophysics*, **47**, 203–221.

[60] Funke, H., Chukalina, M., and Scheinost, A.C. (2007) A new FEFF-based wavelet for EXAFS data analysis. *J. Synchrot. Radiat.*, **14**, 426–432.

[61] Ravel, B., Slimmer, S.C., Meng, X., Wong, G.C.L. and Lu, Y. (2009) EXAFS studies of catalytic DNA sensors for mercury contamination of water. *Radiat. Phys. Chem.*, **78**, S75–S79.

[62] Kleywegt, G.J. and Jones, T.A. (1998) Databases in protein crystallography. *Acta Crystallographica Section D*, **54**, 1119–1131. HIC-Up (http: //xray.bmc.uu.se/hicup), accessed 18 February, 2014.

[63] Kelly, S.D., Kemner, K.M., Fein, J.B. *et al*. (2002) X-ray absorption fine structure determination of pH-dependent U-bacterial cell wall interactions. *Geochim. Cosmochim. Acta*, **66**, 3855–3871.

[64] Locock, A.J. and Burns, P.C. (2002) The crystal structure of triuranyl diphosphate tetrahydrate. *Journal of Solid State Chemistry*, **163**, 275–280.

[65] Templeton, D.H., Zalkin, A., Ruben, H. and Templeton, L.K. (1985) Redetermination and absolute configuration of sodium uranyl(VI) triacetate. *Acta Cryst. C*, **41**, 1439–1441.
[66] Calvin, S., Carpenter, E.E., Ravel, B. *et al*. (2002) Multiedge refinement of extended x-ray-absorption fine structure of manganese zinc ferrite nanoparticles. *Phys Rev B*, **66**, 224405.
[67] Tomić, S., Searle, B.G., Wander, A. *et al*. (2004) New Tools for the Analysis of EXAFS: The DL EXCURV Package. *Council for the Central Laboratory of the Research Councils.*